Chapter 6

Additive Manufacturing of 3D Printed Microwave Passive Components

Irene O. Saracho-Pantoja, José R. Montejo-Garai,
Jorge A. Ruiz-Cruz and Jesús M. Rebollar

Additional information is available at the end of the chapter

http://dx.doi.org/10.5772/intechopen.74275

Abstract

This chapter presents a comprehensive analysis of the applications of a low-cost version of additive manufacturing (AM). The technique called Fused Filament Fabrication (FFF), which makes use of plastic as raw material, is explained in the context of its applications to the microwave waveguide engineering field. The main advantages of this technology include the promptness to print models, the variety of feasible geometries, and specially the reduced cost. The main limitations are also explained. Two important applications are considered: (1) rapid prototyping of complex devices and (2) manufacturing of fully functional devices. The former is relevant to get a more realistic perspective of the actual geometry in computer-aided designs, as shown in several examples. It also helps to forecast possible issues in the fabrication process that the computer sometimes fails to detect at the design stage. In the latter case (2), the subsequent and necessary metallization of plastic devices is also addressed. Several examples of state-of-the-art passive waveguide devices are presented, including waveguide filters, a diplexer, a branch-line coupler, a load or horn antennas, which have been printed, metallized, and measured. The results show the potential of three-dimensional (3D) printing and provide a different insight into this innovative technology.

Keywords: additive manufacturing, 3D printing, waveguide, prototyping, filter, diplexer, coupler, horn antennas

1. Introduction

The idea of Additive Manufacturing (AM) has turned out to be a great disruption in the recent years. In this new technological paradigm where speed, adaptability, or sustainability plays a

very important role, the use of new materials and manufacturing techniques is gaining momentum. Consequently, the idea of three-dimensional (3D) printing has affected many different fields in ways previously unconceivable, and microwave engineering is not an exception.

Some of the main advantages of 3D printing include the promptness to manufacture a model, the ability to produce personalized items, the great variety of available geometries, or the fast and clearer communication of new ideas. These statements may sound quite unspecific, but they are indeed true for both an engineering company and a jewelry designer. The goal of this chapter is to narrow down those general ideas of how useful 3D printing may be in the context of the microwave engineering field.

Moreover, there is one important issue that has not been mentioned yet: the cost. One of the causes of the versatility of 3D printing is that it can be applied to almost any material, with the correspondent cost variation. However, in this work, the technology is addressed from an extreme low-cost perspective, aiming to reach a large audience.

In brief, the application of low-cost AM to the microwave engineering field is explained in detail through several real-world examples—designed, manufactured, and measured devices—which have been previously reported in the literature. Consequently, the down-to-earth advantages of this technology are not only highlighted but the drawbacks are also analyzed. The aim is to help students and radio frequency (RF) and microwave engineers to discover the full potential of the AM directly applied to their area of expertise.

1.1. What is low-cost additive manufacturing? Historical background

It is not possible to address AM as neither single nor simple concept. As a general description, it may be explained as the addition of materials in layers in order to build an object from a digital model [1]. This object can be made from many different raw materials—from wood or metal to food or human tissues—and therefore a great range of physical processes or technologies are involved. For example, the materials or techniques used to 3D print jewelry may not be the same as the ones used in the architectural field or for biological research. This intuitive idea has been recently standardized [2] leading to seven categories of AM processes [3]:

- Binder jetting: A liquid bending agent is deposited to join powder particles.
- Powder bed fusion: Material powder is melted and fused together by using a laser or electron beam.
- Directed energy deposition: The material—in wire or powder form—is extruded from a nozzle and melted with a laser or electron beam upon deposition.
- Material extrusion: Melted material is extruded from a nozzle and fused together upon deposition.
- Material jetting: Droplets of viscous material (polymers, waxes) are deposited, solidified, and then cured with ultra-violet (UV) light.
- Vat photopolymerization: A vat of resin is selectively hardened with UV light.
- Sheet lamination: Sheets of metal are bound together by using adhesive or welding.

Roughly, there are four main technologies: to extrude, to compact powder, to selectively solidify the material, or to use lamination techniques. The detailed differences and applications of each of them are beyond the scope of this chapter. However, as in any engineering process, cost is a key factor in order to decide which AM process is more relevant in each case.

Low-cost 3D printing is usually related to thermoplastic for obtaining objects through "material extrusion." A common name for this technique is Fused Filament Fabrication (FFF), and it is the most popular technology chosen by private end users.

The 3D printing industry has been in the stage of development for several decades. It started in the late 1980s, yet the technology was only available to professional levels because of the high cost of the equipment [4]. However, the real trigger in the development of low-cost 3D printing is caused by the expiration of FFF patents in 2009 and the rise of the open-source movement, involving both hardware and software. The do-it-yourself philosophy has become very popular and has created the "maker" culture in this technological field. As a final consequence, 3D printing is now available and affordable to masses: having your own 3D printer is worth a few hundred dollars.

Apart from the 3D printer itself, other components are needed likewise low cost. The machine works by extruding a heated thermoplastic filament from a nozzle. The plastic is usually acrylonitrile-butadiene-styrene (ABS) or polylactic acid (PLA), both provided in spools [1]. As a reference, the latter may cost approximately 25 $/kg. Finally, the software needed to process the digital models is open source [5].

Regarding the plastic choice, both ABS and PLA present different characteristics. The latter is the one used to manufacture the devices presented in this work, and it is also the preferred option for low-cost 3D printers because of its bioorganic origin. PLA does not usually require a heated bed print and presents less warping than ABS, apart from being more environmentally friendly.

1.2. Advantages and applications of low-cost AM in microwave engineering

As it has been previously mentioned, 3D printing and its low-cost version are used in a great variety of fields. In addition, it is interesting to analyze the main uses of this technology for the microwave engineer to get the maximum throughput.

In this work, when microwave or RF engineering is considered, it is mainly referred to passive waveguide devices. In this way, two main applications can be distinguished: prototyping and manufacturing. Since the material used to build the device is plastic, a subsequent metallization process may be conducted. In the former case, the device would remain as a model; whereas in the latter it can be used for real applications.

When 3D printing for prototyping is considered, the main goal is to reach a clearer communication in the discussion between the microwave designer and the professionals of the manufacturing workshop. There is a saying that an image is worth a thousand words, with the AM taking this a step further by considering that a 3D physical model is worth a thousand 2D representation. The microwave engineer may sometimes design some difficult geometries and then another party may take care of the manufacturing. If an initial prototype is available for discussion, it may be easier for the mechanical engineer to identify the main structural challenges as well as

having a global vision of the whole device itself. The engineer may also realize that some parts of the design could be improved or modified. Of course, computational 3D models are normally used, but with low-cost 3D printing, a full-scale model is available almost instantly. AM becomes a tool to gain a deeper understanding throughout the design process.

Besides, the availability of real models may be useful for another application full of potential: education [6, 7]. Models provide outstanding intuition without replacing theoretical results. Students have started to use computational tools to complement their academic training, and AM brings that to a whole new level. After studying the theory, the students are capable of handling state-of-the-art filters, antennas, orthogonal mode transducers (OMTs), or power combiners in the laboratory.

For these prototyping applications, the designed devices are not intended to work, that is, the model can remain a dummy with no further utility. However, in order to obtain a device with proper electrical response, it is mandatory to include metal in the process. When metal is the raw material used to 3D print the model, many advantages of AM appear more evident. For instance, unfeasible geometries by traditional means such as computer numerical control (CNC) milling may be achieved. Besides, there is a saving in consumed material, making the whole process more sustainable. Yet to combine those advantages with plastic 3D printing represents a bigger challenge, that is, low-cost.

Metallization of the plastic device may be done by different means, but the specific approach followed in this work is metallic paint. For some devices, the results show that it is acceptable to use the final devices in real communication systems, whereas others eventually require some modifications. In spite of that, they both open up another possibility within the educational field. If prototyping offers the possibility of *touching* microwave devices, manufacturing allows performing a full design process at a bachelor or master's level.

In RF courses, the first step is usually to acquire a theoretical background. In the best-case scenario, students are later asked to design a device that must fulfill certain specifications and obtain a simulated response through software tools. However, experimental validation is sometimes avoided or limited due to the lack of resources. Consequently, students may measure or test specific devices intended for that use but very rarely do they test what they have done themselves. Low-cost 3D printing changes this paradigm and allows students to conduct a full design process: from the initial design stage to the measurement of their own models [6]. The physical structure may be printed in few hours once the design is completed. Therefore, it is possible to verify whether the real-measured response matches the expected one, causing a deeper engagement in the courses. Another advantage is that each student may design their own model with different specifications, as well as facing the real challenges of real-life manufacturing. Fabrication entails restrictions that must be borne in mind: students must design a physically achievable device, something that may be forgotten when the design process ends with a simulated response in the computer.

Finally, the common denominator in both cases is that the low-cost approach makes the technology accessible to all kinds of engineering environments: from individuals to small research groups instead of just large companies or high-level laboratories. The prototypes or functional devices are promptly manufactured within hours after being designed for less than 25 $ each.

2. Prototyping

Prototyping is one of the applications of additive manufacturing in many diverse fields, including also microwave engineering. In recent years, there has been a notorious increase in the amount and quality of computer-aided design (CAD) tools for design and visualization purposes. These developments are of great help for designers and engineers, but, at the end, physical realization gives an irreplaceable insight: this is the context where AM plays a key role. Moreover, when the design process moves to the manufacturing stage, it is mandatory to pay special attention to mechanical and structural issues.

Since the printed prototypes are only relevant from a mechanical perspective, plastic is a suitable material with no further metallization needed. The manufactured geometries are feasible for real devices thanks to complex and expensive fabrication techniques such as CNC milling. However, FFF allows obtaining a model in few hours.

Figures 1 and **2** represent two examples of prototypes of state-of-the-art waveguide devices. They are Ku-band power combiners with 8 and 16 ports, respectively. The top part in **Figure 2** is a circular TE_{01} mode converter which has already been presented in [8] together with its printed model to forecast any problems in the ongoing CNC milling fabrication process.

Figure 3 shows a model of a diplexer intended to work in Ka-band made out of two band-pass filters with elliptic response. This kind of design is suitable for satellite applications due to its outstanding electric performance and robust and compact structure [9].

Finally, other manufacturing techniques may also benefit from low-cost additive manufacturing. One example appears in **Figure 4**, where the different pieces of an ortho-mode transducer (OMT) based on the turnstile junction, working in W-band are presented, allowing to anticipate and to discuss any issue in the final manufacturing. In this case, the final fabrication technology was layered SU-8 photoresist, and the plastic pieces allow seeing the different layers in which the structure is divided.

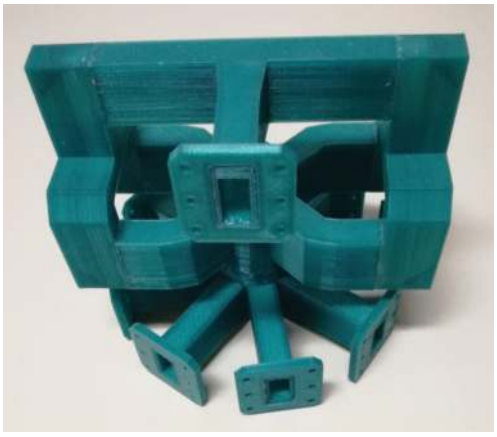

Figure 1. 3D–printed prototype of a Ku-band 8-port power combiner.

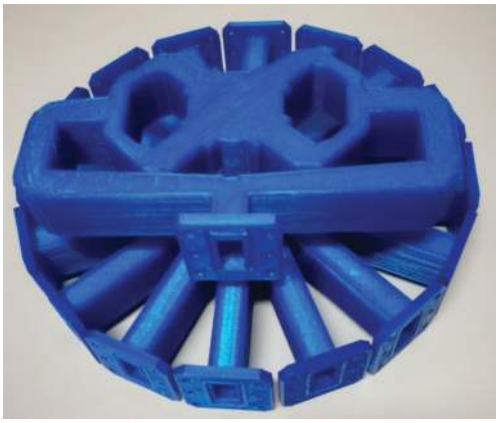

Figure 2. 3D–printed prototype of a Ku-band 16-port power combiner.

Figure 3. Printed model of a Ka-band diplexer with two band-pass filters with elliptical response.

Figure 4. Printed layers of an ortho-mode transducer (OMT) based on turnstile junction, working in W-band.

In all these cases, very complex designs with reduced price are rapidly available. Some geometries involve many difficult details, even with the available visualization tools nowadays. These cases are therefore good examples of how 3D printing can help to reach a clearer communication between the different teams involved in an engineering product.

3. Manufacturing of waveguide devices

After addressing the first application of low-cost 3D printing in the microwave field, another step is introduced. Now, the printed devices are meant to be measured, and therefore, they have to be metallized first. These two requirements set a frame of limitations, which confine the usability of this technology—at least the low-cost version—and are crucial to understand the electrical responses of the devices presented later in this chapter.

First, the three main restrictions are thoroughly explained. Then, a full set of waveguide devices and two horn antennas are presented. They cover from relatively simple straight sections to fully operational devices such as a waveguide diplexer with challenging specifications. They try to push low-cost 3D printing to its limits, also in terms of frequency and bandwidth.

3.1. Limitations of low-cost 3D printing process

The main drawbacks of low-cost 3D printing when manufacturing fully functional devices may be summarized as follows: the working frequency, the metallization process, and the structural issues.

3.1.1. Dimensions

The first one is intrinsically related to the dimensions of the design and the printing accuracy, that is, the layer height. In a normal low-cost machine, the minimum value is ±0.1 mm. It marks the minimum variation of dimensions that can be built, and, therefore, it establishes an upper limit for the working frequency. It is unrealistic to print devices with working band above 15 GHz. Besides this limit, this issue becomes even more evident when dealing with sensitive devices, where a tiny variation of dimensions leads to a very different electrical behavior.

Printing accuracy is also related to the achievable matching losses in a waveguide device. In an experiment performed with printed 50-mm-long WR75 waveguide sections such as the one in **Figure 5**, the matching level is similar for the waveguides regardless of the paint they are covered with: around 20–25 dB in Ku band, as it appears in **Figure 6**.

All things considered, this limitation is probably the easiest to deal with. There is a quite clear limit regarding frequency, and computational design tools are of great help to account for precision. That means that before obtaining the final model of the device, all geometrical dimensions should have the number of decimal digits in agreement with the printing accuracy.

3.1.2. Metallization

The second drawback includes all the aspects related to the metallization process. As it has been mentioned, it is imperative to cover the inner surface of the printed waveguide devices with metal paint, in order to confine the electromagnetic energy within the structures. Consequently, the devices cannot be printed as a single piece, as it would be desirable, but they have to be printed in separate parts instead. Their inner part must be accessible for painting and that may limit the feasible geometries in some cases. This may be seen as damaging one of the biggest advantages of 3D printing, yet it is a trade-off and from this perspective the total cost is very low.

Figure 5. 3D printed WR75 waveguide section ready to be measured.

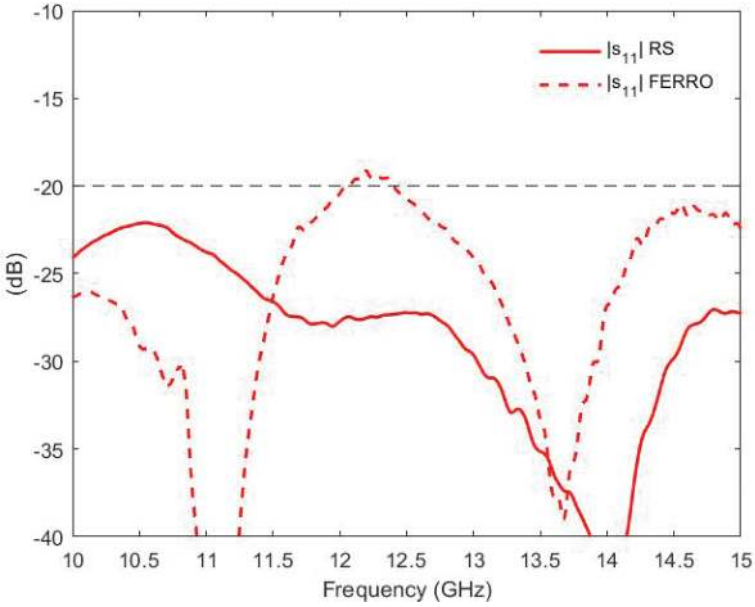

Figure 6. Measured matching level of 3D printed 50-mm-long WR75 waveguide sections covered with RS and Ferro paint.

Besides this trade-off, it is crucial to find a metal-loaded paint with good quality and a reasonable price. It is a hard task, since the obtained conductivity is not very high and depends on frequency. It causes relevant insertion losses which may clearly deteriorate and even *hide* narrow-band responses. For this work, several commercial paints were tested before manufacturing complex devices. The first one was a repair kit for rear windscreen defoggers [10]. The conductivity value was claimed to be high due to the silver content, yet no specific value was provided. Conducted tests showed high insertion losses, and thus the paint was left out.

Two other metal paints with silver content, supplied by Ferro [11] and RS [12], were considered. In both cases, the conductivity was provided, although the value given was for DC. In the same experiment with the waveguide sections, insertion losses were also analyzed. Their provided nominal conductivity was $\sigma = 10^5$ S/m (RS) and $\sigma = 1.6–5 \cdot 10^6$ S/m (Ferro), which is one or two orders of magnitude below silver conductivity itself ($\sigma = 6.3 \cdot 10^7$ S/m). However, the effective conductivity is better for RS paint in Ku band, as shown in **Figure 7**. Such results are critical and RS paint is the natural choice to metallize 3D–printed devices. Its price was approximately 60 $/20 g at the time of the experiment. The effective conductivity used in subsequent simulations was $\sigma = 5 \cdot 10^4$ S/m.

Metallization was performed by hand and each section was painted twice to ensure a homogeneous layer with no air gaps or drops of paint remaining. In fact, conductivity is not the only issue affecting the response. That may explain why the effective conductivity of RS paint is higher than Ferro, although for nominal values it is the other way around. The density of the paint may play an important role as well. For instance, the Ferro paint is not very thick and therefore it may not be well absorbed by the plastic, resulting in a defective metallization process.

The problems derived from the metallization process are not only related to the paint itself. Since the waveguide structures need to be split, the eventual alignment turns out to be critical. The different parts must be joined back together and glued, since any misalignment would cause a significant variation in the electrical response. Extra parts such as fastening pieces may also been used, as mentioned later in the chapter.

Finally, the influence of the plastic spools may be worth mentioning, since the quality of the plastic affects how well the paint is slicked to the plastic. Plastic characteristics may vary from one supplier

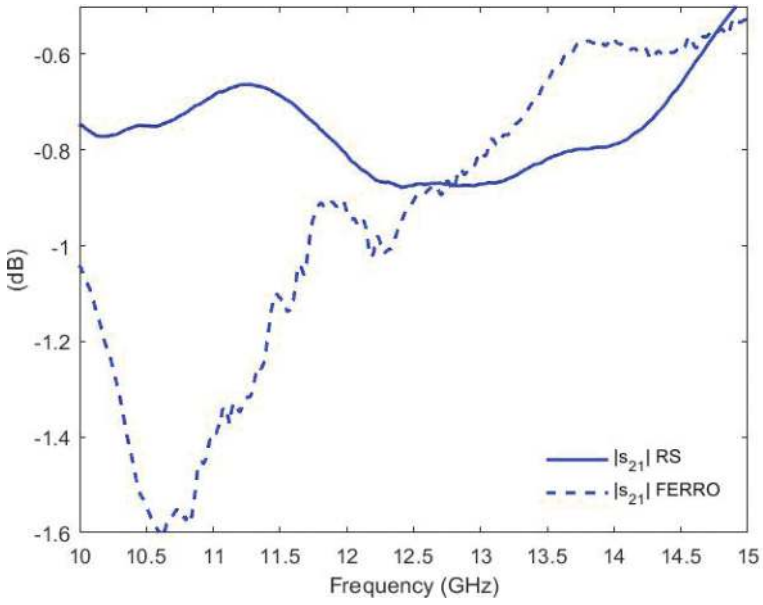

Figure 7. Measured insertion losses of 3D printed 50-mm-long WR75 waveguides painted with RS and Ferro paint.

to another, and even between spools or colors. Consequently, the plastic may absorb the paint differently. The behavior with humidity or temperature variations may vary as well. As a reasonable practice, it is recommended to maintain the material supplier in order to try to reduce such variations.

3.1.3. Structure

This last limitation is more specific for passive waveguide devices such as filters, diplexers, or couplers. Its effect in the horn antennas presented later is much less important.

Since the structures must be split into pieces to metallize them, two main possible divisions are considered: E-plane or H-plane (**Figure 8**) [13]. The former consists in splitting the structure into two identical halves, following the so-called E-plane approach (cutting in the plane where the E-field is maximum), whereas the latter separates the structure in body and cover. Trying to determine the best approach, some experiments were conducted.

Figure 9 shows the insertion-loss level of 40-mm-long WR75 waveguide sections covered with the same paint. The H-plane structure presents higher losses. That may be explained by considering problems assembling the structure or misalignments. H-plane structures are more sensitive

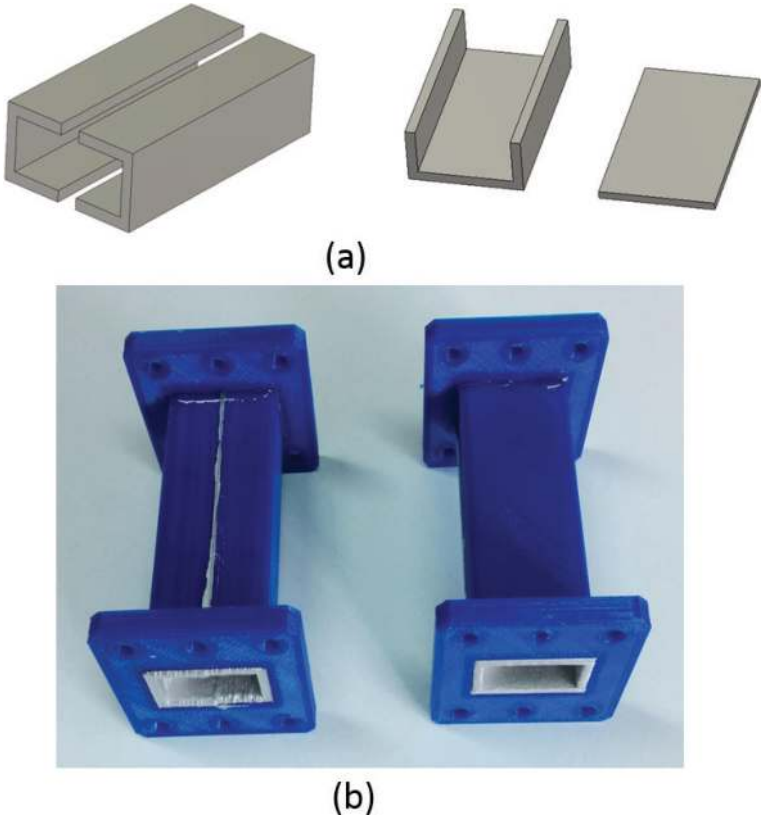

Figure 8. (a) CAD model and (b) 3D printed E-plane and H-plane structures at left and right, respectively.

to this kind of issues, since a perfect contact between the body and the cover must be reached. In traditional mechanizing, screws are used to tackle this problem, but a tiny air gap in 3D–printed designs is almost unavoidable. Besides this, there might be a bending of the top layer.

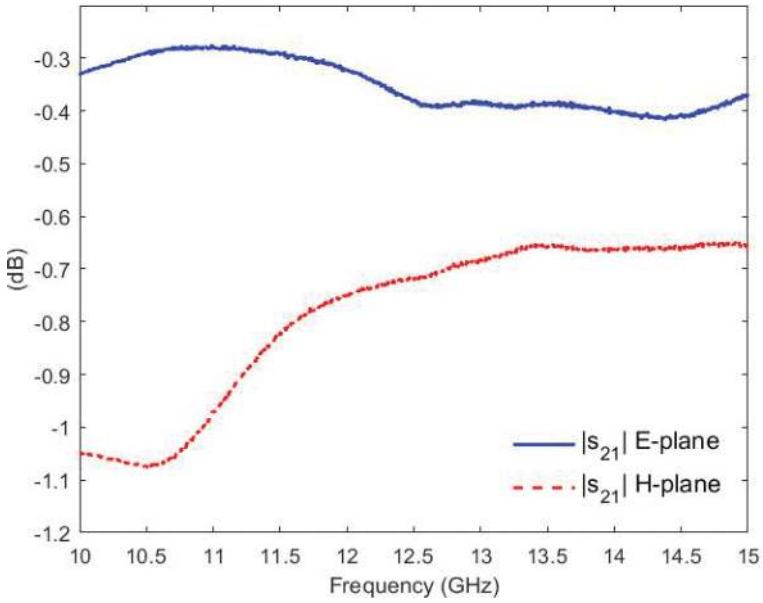

Figure 9. Insertion losses for WR75 waveguide sections (E-plane and H-plane).

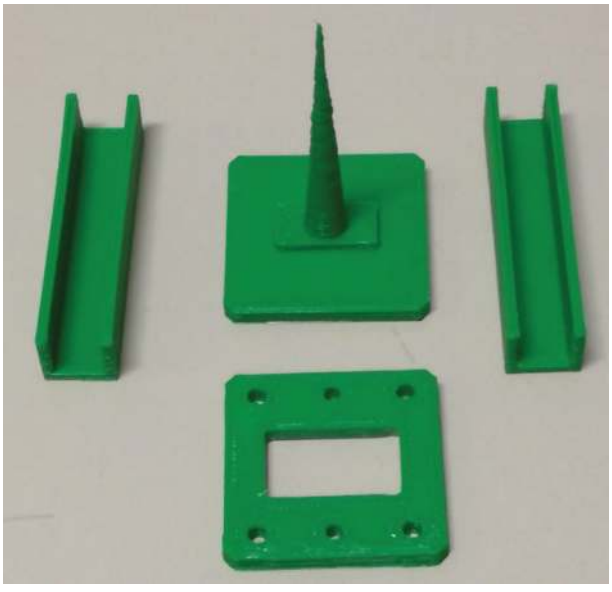

Figure 10. PLA-printed pieces of the waveguide load before being covered with the graphite powder.

On the other hand, E-plane structures show lower losses since they do not depend that much on the assembling. This is due to the absence of currents along the cutting plane. Consequently, dividing the structure into two halves is the best way to proceed and that is how it has been done in this work.

3.2. 3D printed devices: experimental results

3.2.1. Waveguide load

The first waveguide structure to be characterized is a load for Ku-band. It is split in several pieces, printed in plastic, and subsequently covered in Graphite 33 [14], a graphite lacquer for conductive coatings which shows a good electrical conductivity due to the high level of pure and fine graphite powder. Both inner and outer surfaces are coated. The two stages of the manufacturing process appear in **Figure 10** and **Figure 11**. The former shows the different parts of the load before coating them with the graphite powder, whereas the measurement setup with the assembled load appears in the latter.

The matching response is shown in **Figure 12**, with a matching level better than 21 dB in the whole band. Such result is equivalent to some commercial short waveguide loads working in the same band [15].

3.2.2. Waveguide section

After the loads, a simple two-port device is tested: a straight waveguide section. Although some of them were tested to decide between the different paints or the most suitable way to cut the structure, the S-parameters of a 3D–printed 50-mm-long WR75 waveguide section are presented in **Figure 13**. Perhaps a remarkable fact is the lack of symmetry between S11 and S22, which is due to the inherent asymmetries associated to the 3D–printing process. However, the matching level agrees with previously obtained values, as well as the insertion losses in Ku band.

Figure 11. Measurement setup of the waveguide load.

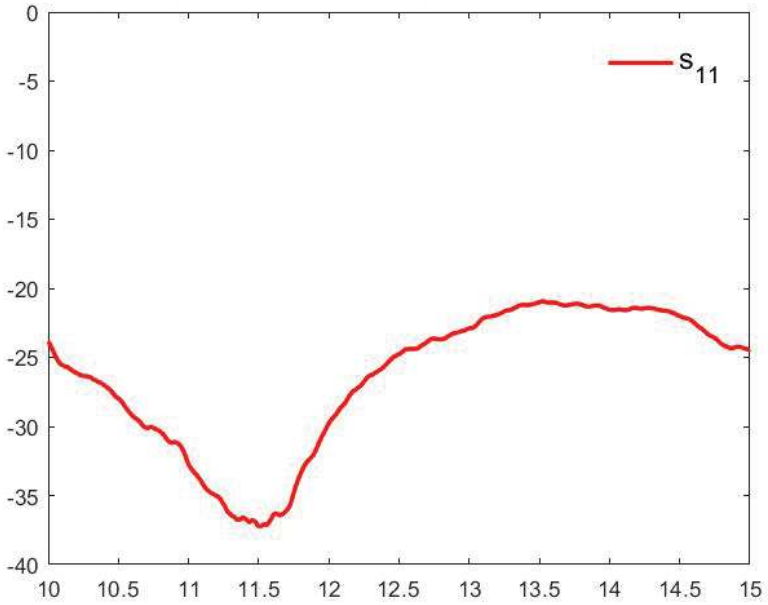

Figure 12. Matching response of the 3D printed load.

3.2.3. Filter: low-pass, high-pass, band-pass

After having analyzed simple waveguide elements such as the load or the straight section, a very challenging passive device is addressed. Filters are key components in the microwave field and their main purpose is to allow a good transmission of desired signals while rejecting the unwanted ones. Depending on their response, they are classified in low-pass, high-pass, band-pass or band-stop filters. In this work, examples of the first three groups are implemented using 3D–printed rectangular waveguides. The results were first presented in [6, 7, 16, 17]. For these and all the other passive devices, the mode-matching technique [18] has been the design tool, whereas Microwave Studio CST [19] has allowed performing the simulations including manufacturing effects.

3.2.3.1. Low-pass filter

Low-pass filters implemented in waveguide technology are based on corrugated structures. The different impedances caused by the varying height of the sections lead to rejection at higher frequencies. In this case, an eight-order low-pass filter with four corrugations has been designed and presented in detail in [6, 17]. It is an E-plane structure. The working bandwidth is from 11.9 GHz to 12.2 GHz. Specifications include 28-dB matching level and rejection higher than 50 dB from 13.75 GHz to 14 GHz. These requirement levels and the frequency bands are typical of satellite telecommunication systems in Ku band and therefore very demanding for low-cost 3D printing technology.

The printed parts of the filter and the assembled structure are presented in **Figure 14**. The most important part of this device is the corrugation width. In this case, it is set to 2.5 mm considering

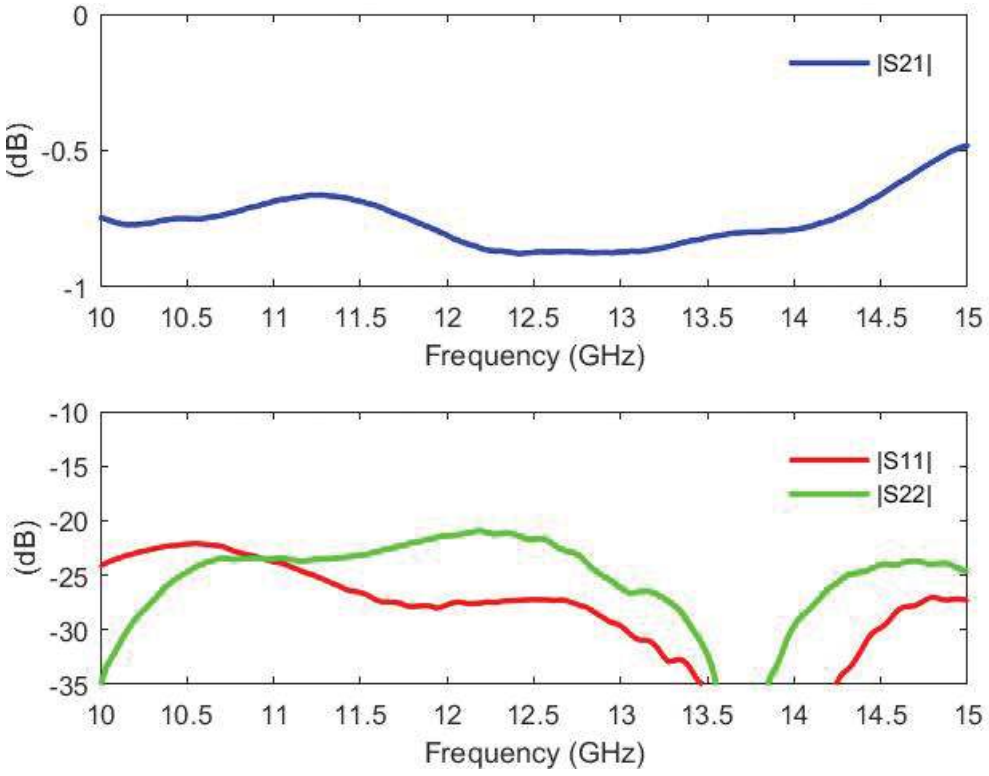

Figure 13. (a) Reflection and (b) transmission S-parameters for a printed WR75 waveguide section.

the printer accuracy. Besides this, it has been possible to avoid input/output transformers, that is, the filter height corresponds to the standard WR75. Consequently, insertion losses have been reduced as much as possible. Finally, it is very important to reach a perfect alignment.

The measurement setup is presented in **Figure 15** and the results are shown in **Figure 16**. The main characteristic of the measured response is that it is wider than the simulated one. In addition, the matching level does not reach the intended level, yet it agrees with the aforementioned limits of the technology and proves how unrealistic it is to try to get more than 22–25 dB return loss in Ku band with low-cost additive manufacturing.

The rejection response differs from the expected one as well. Since the corrugations are the parts causing the reflection, it may be inferred that some modifications should be introduced in future designs. For instance, wider corrugations would allow a better metallization process and therefore a potentially better response. However, it would cause a larger structure with more sections and more insertion losses, which are now around 1.8 dB.

3.2.3.2. High-pass filter

The next design was also included in [6, 17]. It is a high-pass filter based on a waveguide section under cutoff with stepped taper for matching at both input and output ports. The requirements

http://dx.doi.org/10.5772/intechopen.74275

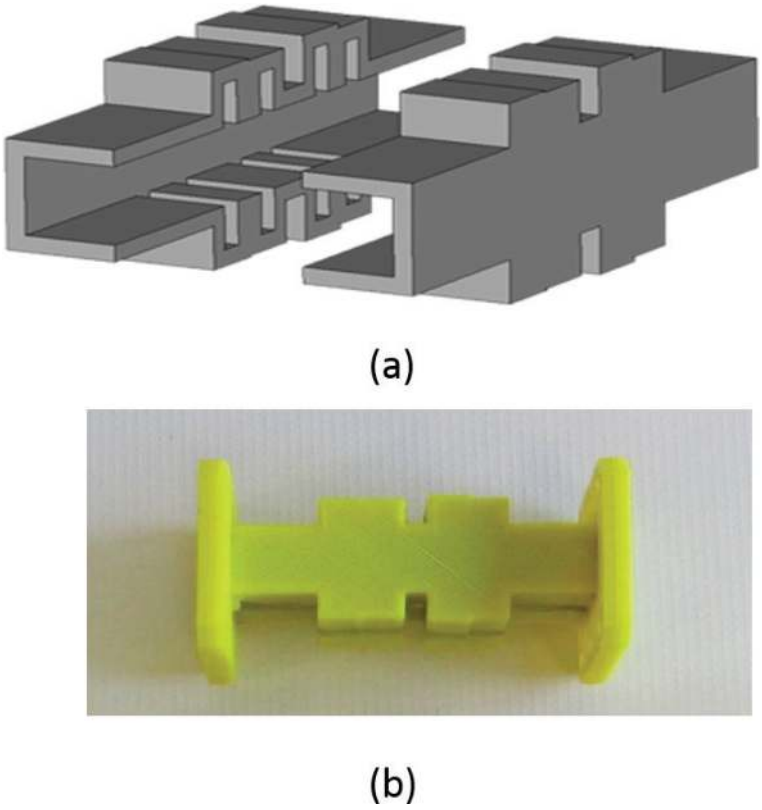

Figure 14. (a) CAD pieces and (b) assembled low-pass filter.

in terms of return-loss and rejection level are the same as in the low-pass filter but for opposite bands, that is, return loss of 28 dB between 13.75 GHz and 14 GHz and rejection greater than 50 dB between 11.9 GHz and 12.2 GHz. From a full-wave design perspective, the filter is an H-plane structure, yet an E-plane implementation has been followed, as shown in **Figure 17**.

Figure 18 shows the measured results. In this case, the filter itself is less sensitive than the previous one; therefore, a quite good agreement is expected and achieved. The matching level is even better than the usual one.

3.2.3.3. Band-pass filter

The last filter was introduced in [7, 16]. It is a band-pass one, where selective frequency response is directly related to the resonance phenomenon [20]. The process involves high standing waves and electromagnetic field intensities, and, therefore, insertion losses are expected higher than in high-pass or low-pass filters.

The band-pass filter in **Figure 19** is a third-order Chebychev filter. The figure shows both the CAD layout and the fully assembled structure. Inductive irises are used to couple between cavities. It is centered in 12 GHz and the bandwidth is 600 MHz. Return losses were specified to be 23 dB.

Figure 15. Measurement setup for the low-pass filter connected to the VNA.

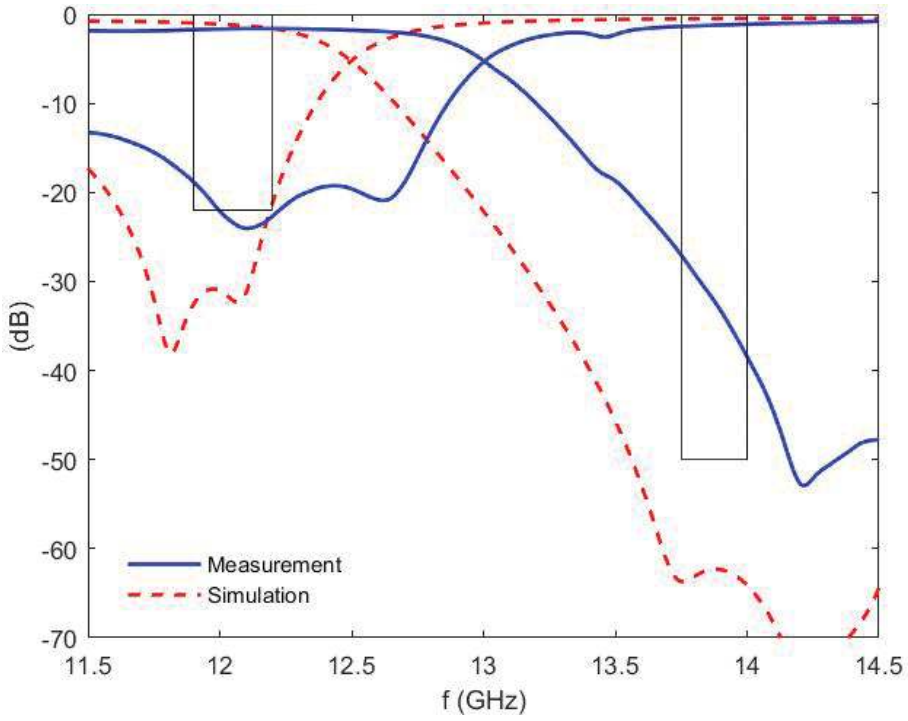

Figure 16. Measurement and simulation results for the low-pass filter.

Figure 20 shows the measured response together with the simulation. The effective conductivity has been considered in the simulations. The matching value is reduced in the 3D–printed model, yet both responses are very close. It shows good agreement with the mean value for 3D–printed waveguides in Ku band. Besides, insertion losses are 1.3 dB at the central frequency.

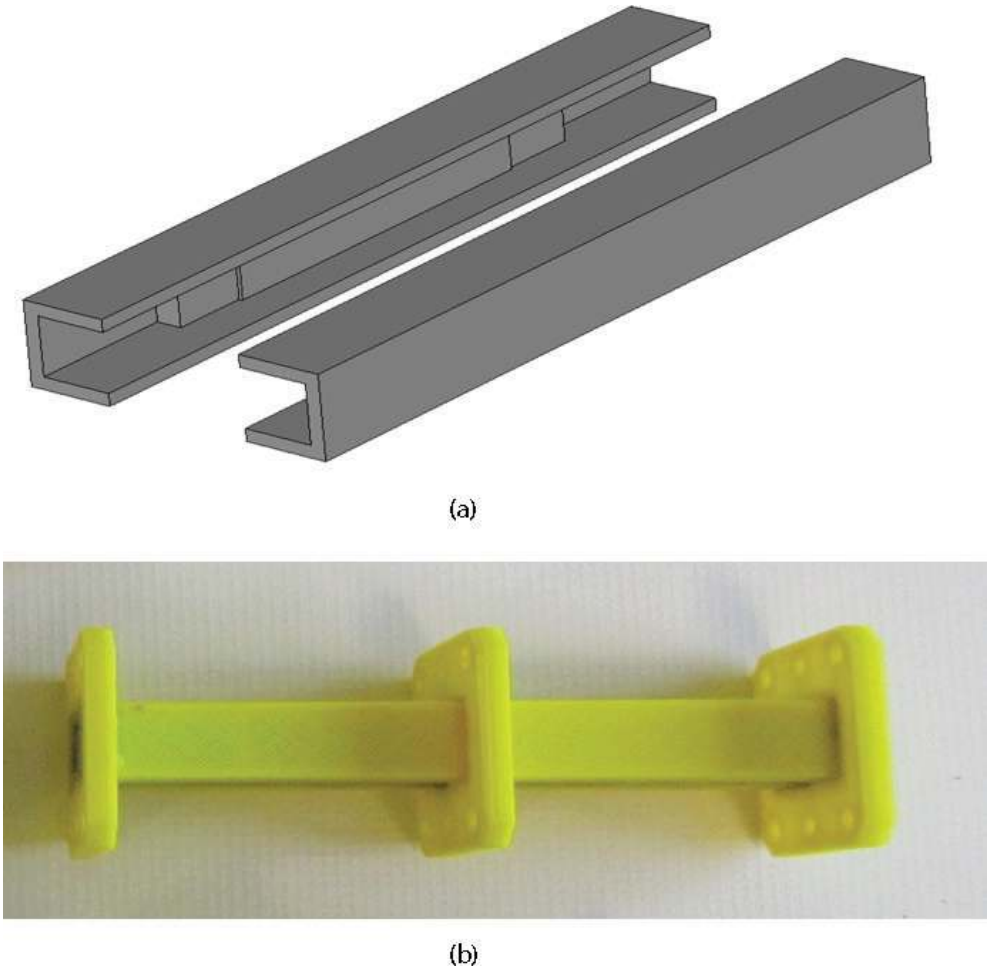

Figure 17. (a) CAD pieces and (b) assembled high-pass filter.

3.2.4. Diplexer

A more complex device is now presented: a diplexer, which is also included in [7]. It is a passive microwave device formed by two filtering structures joined by a three-port junction. Its main application is the use of a single antenna for both transmission and reception in communication systems.

For this design, real satellite communications specifications are used. The passbands are 11.9–12.2 GHz for reception and 13.75–14 GHz for transmission. Return losses and out-of-band rejection are included in the specifications. The former is around 22 dB, whereas the latter is required to be more than 50 dB in complementary bands. For such requirements, different implementations may be used: two band-pass filters or a low-pass combined with a high-pass filter. In this case, the second approach is used since it is the implementation with less insertion losses.

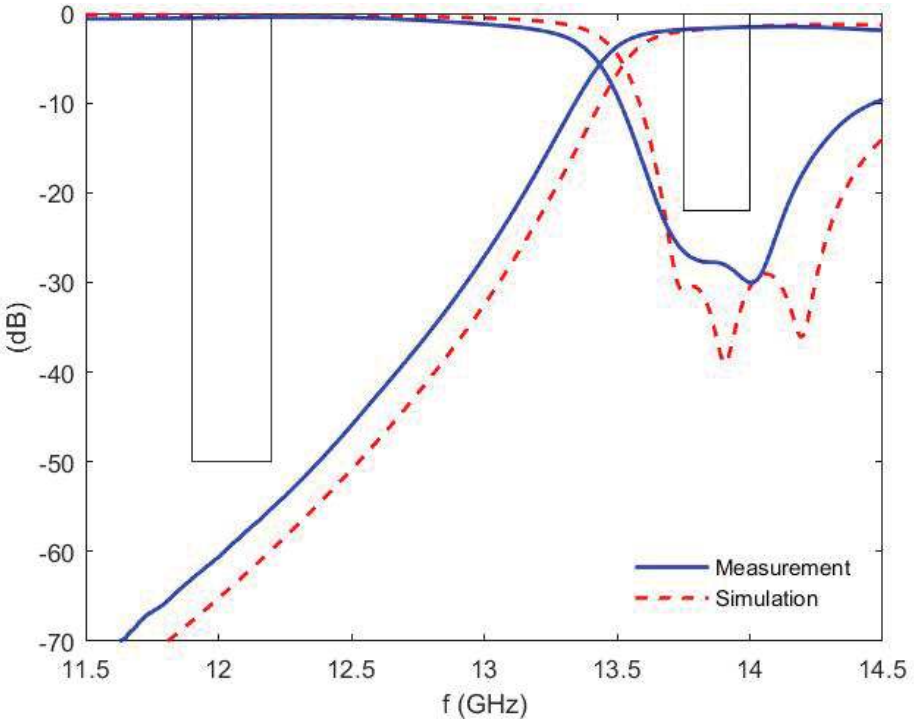

Figure 18. Measurement and simulation results for the high-pass filter.

However, the low-pass filter presents some challenges, as mentioned earlier. Again, the corrugations are the most sensitive part. Consequently, they have been made wider than in traditionally manufactured filters, also to have them painted more easily. Corrugations are 4.5-mm wide, which implies more sections to achieve the same electrical response.

Figure 21 shows the development of the diplexer: (a) the layout, (b) the CAD model, (c) one printed half, and (d) the device prepared to be measured. To join the filters, a three-port junction is designed. Moreover, a double bend is included to allow the waveguide flanges to be attached. Finally, a fastening piece has been printed to keep the two pieces close and avoid any possible air gaps.

The diplexer response is presented in **Figure 22** compared to a simulation with losses. Insertion losses are up to 3.5 dB in the passband. The matching level in both channels agrees with the achievable levels with low-cost 3D printing: approximately 20 dB. It is important to highlight that both responses have moved to lower frequencies as a result of possible printing inaccuracies.

3.2.5. Branch-line coupler

Directional couplers are four-port devices in which the power available at the input port is distributed between two output ports [20]. Perhaps the most common ones are the 3-dB couplers, widely used as input/output in balanced amplifier circuits, in beam-forming networks, as power dividers, and so on. In particular, branch-line couplers consist in two shunt

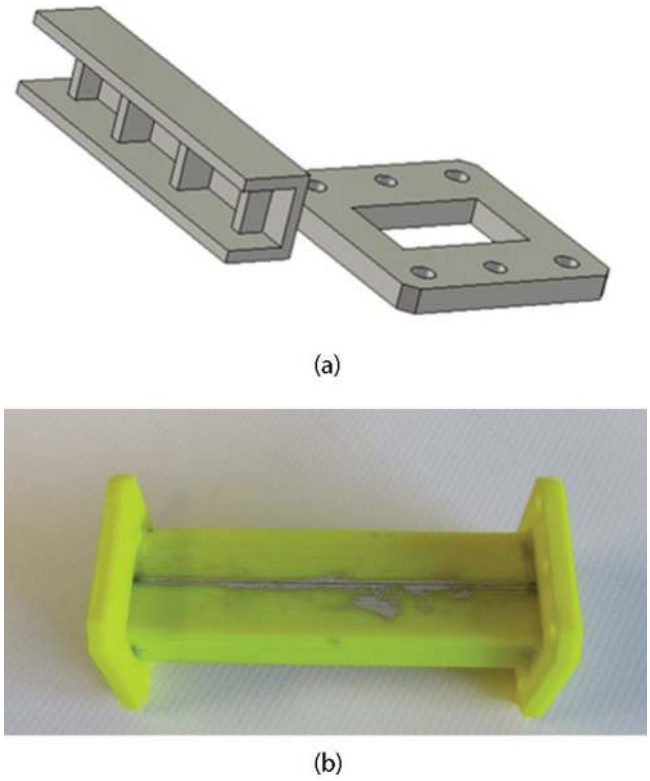

Figure 19. (a) CAD model and (b) assembled band-pass filter.

transmission lines connected by two secondary (branch) lines. They present a narrow bandwidth, although it can be improved by cascading several sections.

A 3-dB branch-line coupler working in Ku band has been designed and the results presented in [7]. Aiming to achieve a broad bandwidth, five branches have been designed. Isolation and matching levels are intended to be 25 dB in the working band. **Figure 23** shows the designed device from the simulation model to the measurement setup. Two double bends have been added to the coupler in order to attach the standard WR75 flanges.

The experimental response is shown in **Figure 24**. In terms of matching and isolation, the results are very satisfactory. The former is greater than 20 dB between 11 GHz and 14 GHz, although if the bandwidth from 11.5 GHz to 14 GHz is considered the matching value results to be greater than 25 dB. The isolation reached is very high as well, considering the limitations of 3D printing. From 11 GHz to 14 GHz, it is better than 24 dB.

The response of the printed branch-line coupler in terms of power coupled to each output port is evaluated on the enhanced part of **Figure 24**. The measurements are compared to a full-wave simulation including losses. They are lower in the transmitted port (P2) than in

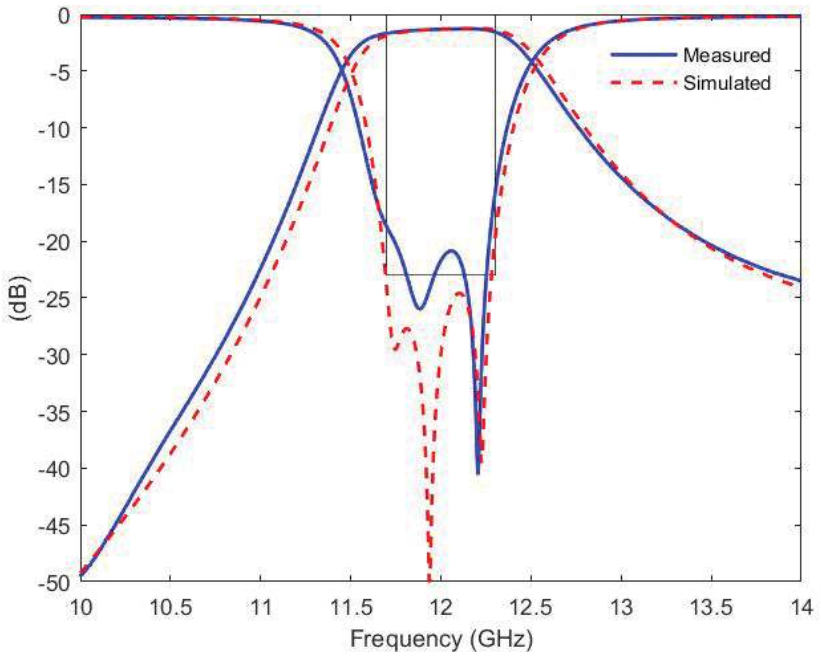

Figure 20. Measurement and simulation results for the band-pass filter.

the coupled one (P3), although the former has a double bend attached. It may be explained by considering that the coupled signal passes through the branches on its way to the output port. Moreover, misalignments are likely to happen, particularly in the small posts among the branches. They are the smallest part of the design, as well as the most sensitive one, as it happened with the corrugations in the low-pass filter.

3.2.6. Horn antennas

The two horn antennas [21] presented in this work fulfill standard horn specifications, according to available commercial models working in the same band, like the Flann horn in [22]. Their gain reaches 15 dBi at the center of the Ku band. The first one is a classical pyramidal horn, whereas the second one has a rectangular aperture and a conformed profile. Their input corresponds to the WR75 rectangular waveguide. The return-loss level for both antennas has been optimized to remain below 20 dB between 10 GHz and 15 GHz. Measurements show a remarkably good agreement with theoretical values, which makes the horns perfectly useful for real communication applications, for instance, indoor systems.

The process is presented in **Figure 25**, together with the CAD design of one horn. The antennas are monolayer structures, that is, only one layer of plastic has been used. Due to this fact, the antennas are extraordinary light—less than 15 gr.—contrary to the weight of traditional

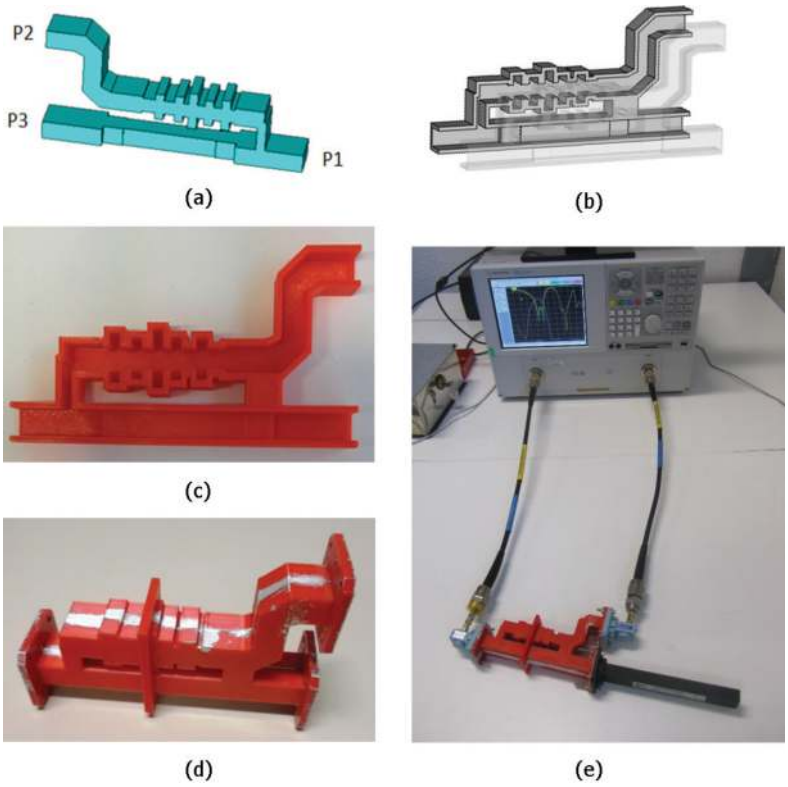

Figure 21. (a) Diplexer layout, (b) half CAD model, (c) one printed half, (d) the device metallized and assembled, and (e) measurement setup.

and mass-produced metal horns. At the same time, they are robust enough and their smooth surface makes it feasible to print them as single structures, instead of splitting them into two parts as it occurred with the previous waveguide devices. It must be highlighted that the printed structures also include the waveguide input (the standard WR75 flange).

The time required to print each horn antenna is approximately 2 hours, notably less than a traditional manufacturing process. Finally, the conformed profile of the second horn would have been very difficult to achieve by traditional means, and it would have required the use of molds. At the end, the total cost of each antenna is approximately 15 $.

Both horn antennas have been characterized in terms of matching level, gain, and radiation patterns. **Figure 26** shows the experimental setup for the pyramidal horn in the network analyzer and the anechoic chamber. The theoretical responses have been obtained with CST. Moreover, the measured gain of the antennas has been compared not only to the simulated response but also to the commercial model supplied by Flann working in the same band.

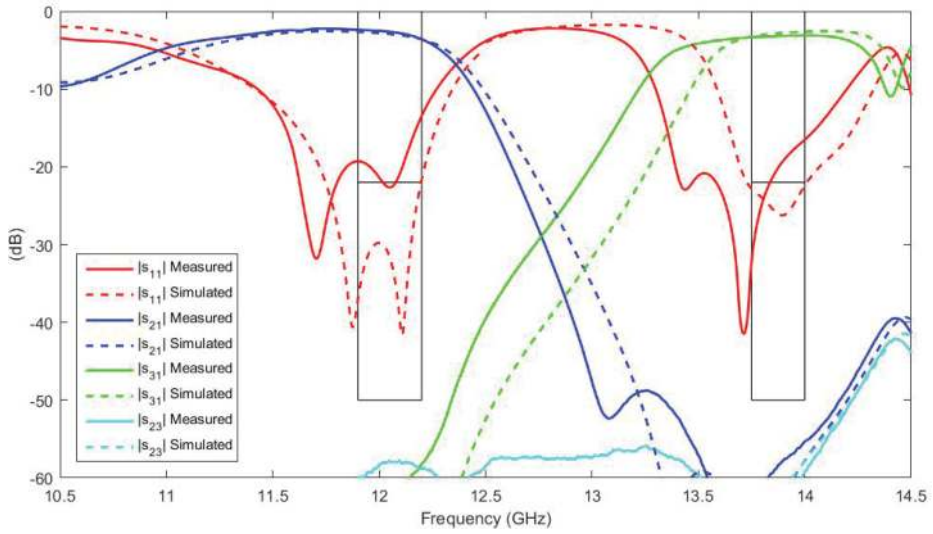

Figure 22. Measurement and simulation results for the diplexer.

3.2.6.1. Matching level

The horn antennas were designed with a return-loss level better than 20 dB between 10 GHz and 15 GHz. The measured responses and the simulated ones ($\sigma = 5{\cdot}10^4$ S/m) are shown in **Figures 27** and **28**. Despite a return-loss level slightly worse than 20 dB between 10 GHz and 10.5 GHz for the conformed horn, the response of the reflection coefficient follows the expected one. However, a small ripple can be observed in both antennas. It is explained by considering multiple reflections due to the inherent roughness and small discontinuities on the walls.

3.2.6.2. Radiation pattern

The normalized radiation patterns in the E and H-plane—elevation and azimuth, respectively—have been obtained at 12.5 GHz for both antennas. The pattern corresponding to the classical pyramidal horn is shown in **Figure 29** along with the simulated co-polar response. The measured response follows the theoretical one very accurately, with a difference in the 3-dB beamwidth of only 1° (**Table 1**). With respect to the cross-polarization level, its measurement is limited by the anechoic chamber used in the horn characterization. In this case, its level is always 30 dB under the main lobe in both planes.

The conformed-profile horn shows a very good response as well, as presented in **Figure 30**. The radiation pattern matches the simulated one accurately and the 3-dB beamwidth barely differs 5° in the worst-case scenario (**Table 1**). Finally, the cross-polarization level remains more than 30 dB under the main lobe in both planes.

3.2.6.3. Antenna gain

The gain over broadband has also been measured for both antennas. The pyramidal horn gain is presented in **Figure 31** compared with the simulated one and the commercial pyramidal horn provided by Flann [22]. It can be seen that the gain of the 3D–printed horn is not as high

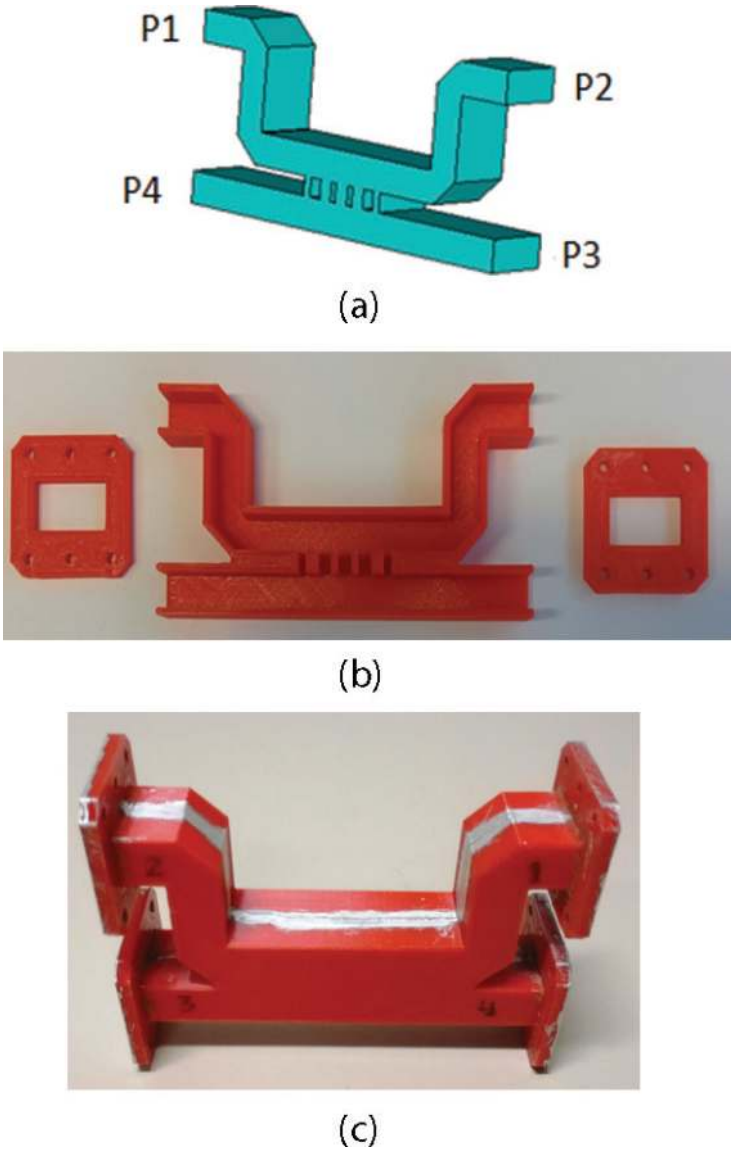

Figure 23. (a) Layout, (b) printed half, and (c) assembled and metallized branch-line coupler.

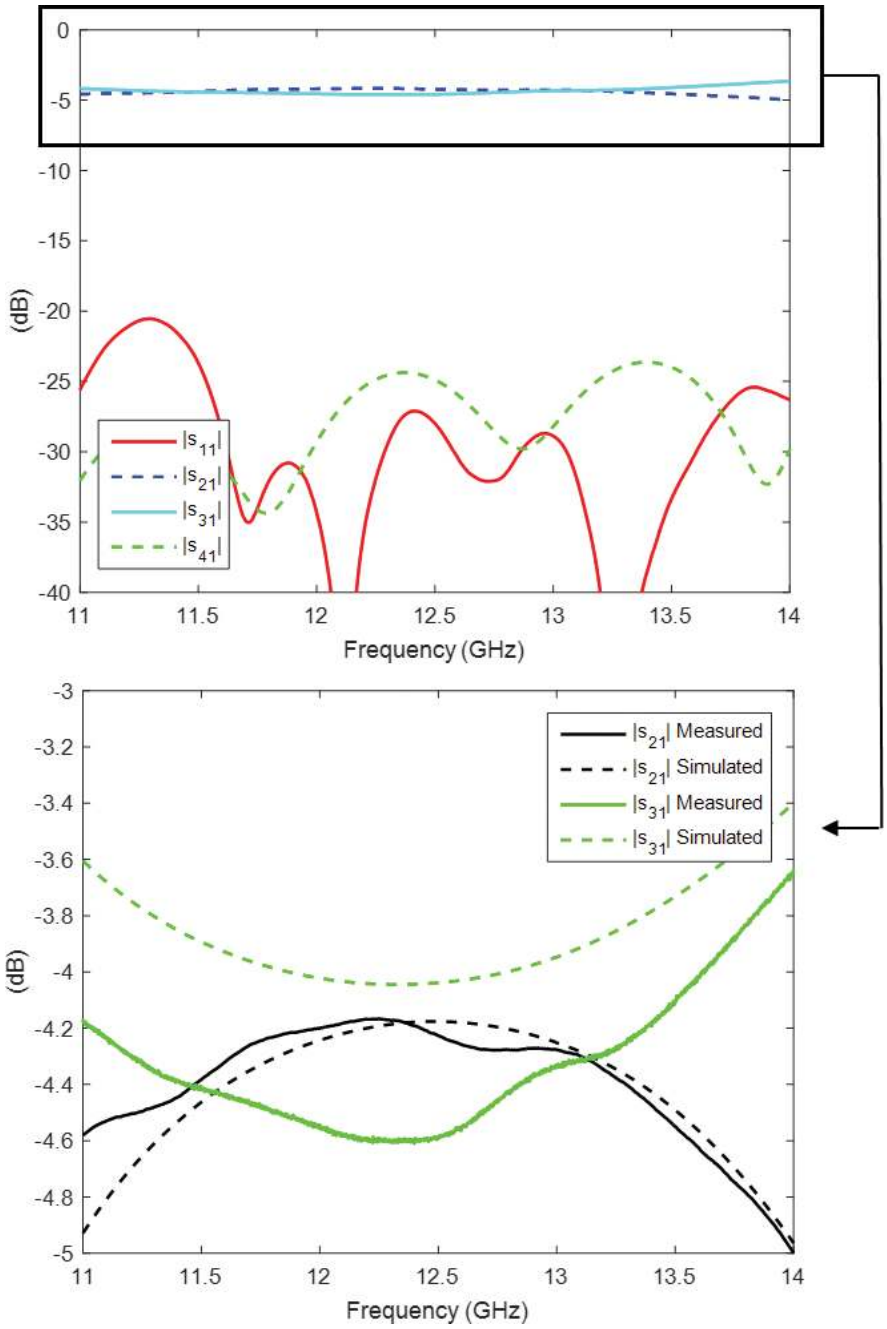

Figure 24. Measurement and simulation results for the branch-line coupler. To the right, enhanced view of the transmission parameters.

http://dx.doi.org/10.5772/intechopen.74275

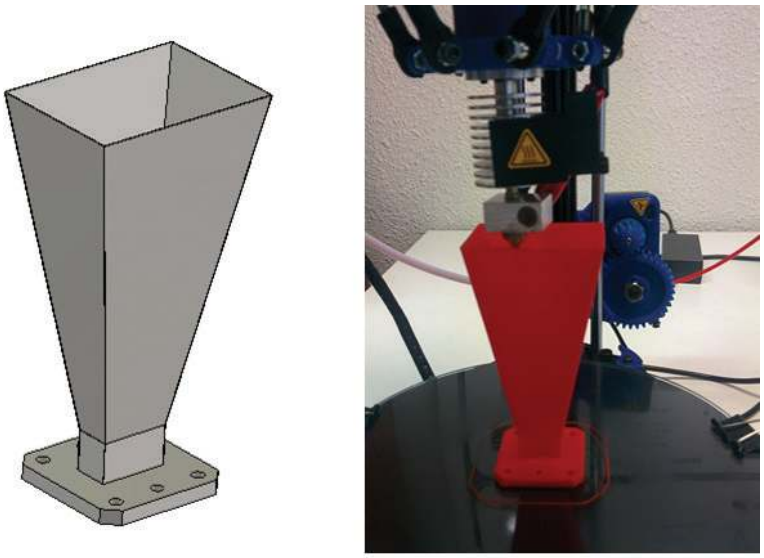

Figure 25. (a) CAD model of the pyramidal horn. (b) Horn antenna being printed with the low-cost PLA 3D printer.

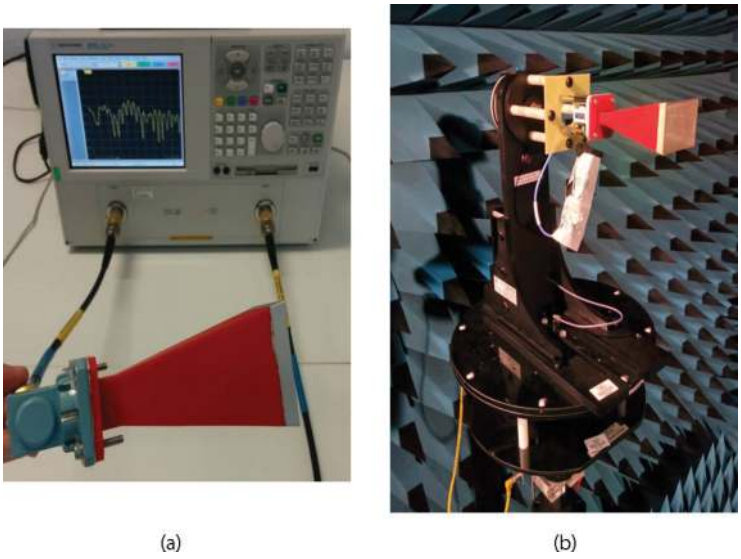

Figure 26. Measurement arrangement for the pyramidal horn in (a) the network analyzer and (b) the anechoic chamber.

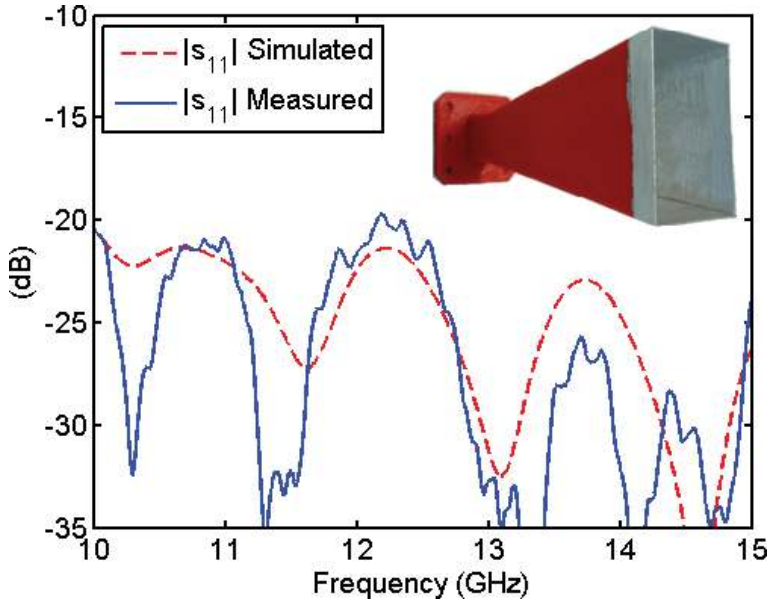

Figure 27. Return-loss level over Ku-band for the classical pyramidal horn. Top right inset: Printed and metallized structure.

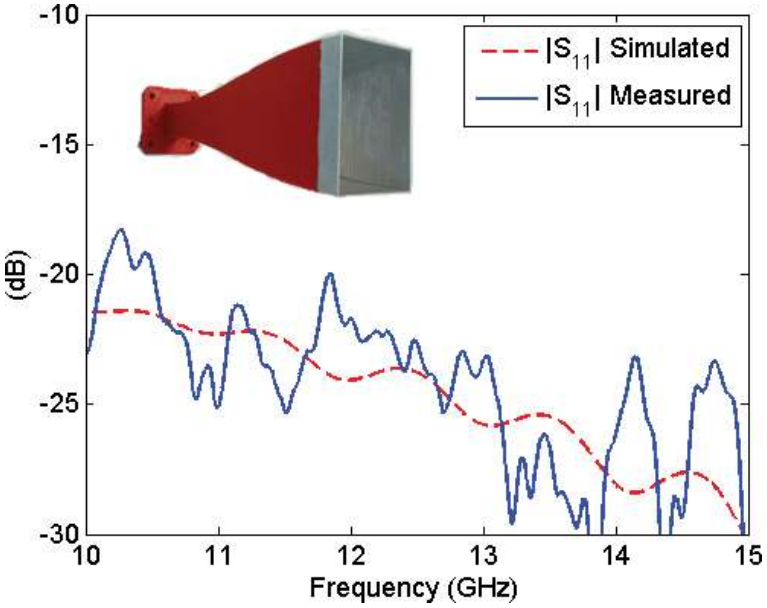

Figure 28. Return-loss level over Ku-band for the conformed-profile horn. Top left inset: Printed and metallized structure.

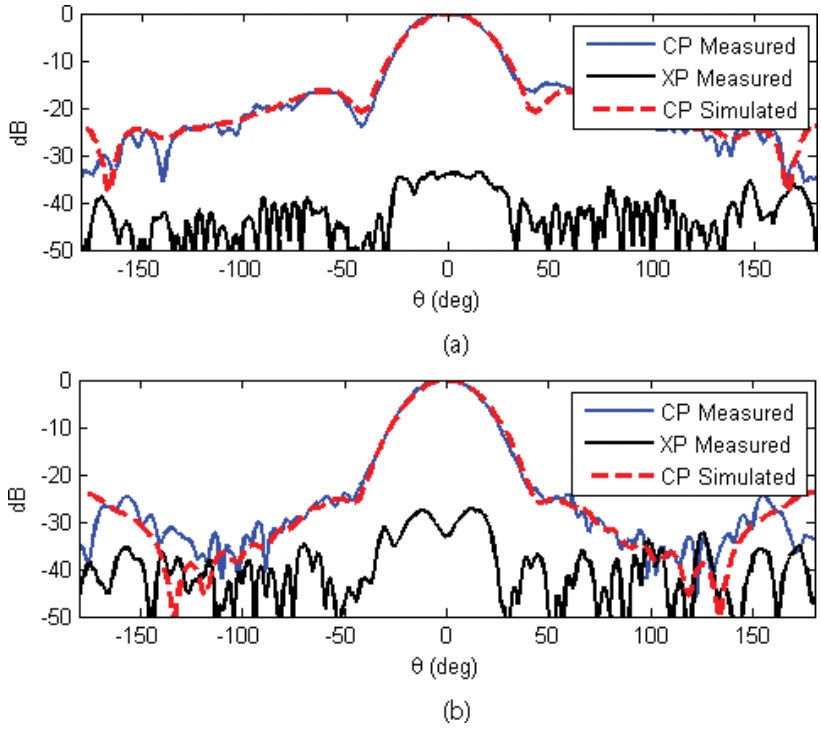

Figure 29. Normalized radiation pattern of the pyramidal horn at frequency 12.5 GHz in (a) E-plane and (b) H-plane.

as the one of the commercial model, with differences up to 1.5 dB, especially in the lower band. There are discrepancies with the simulation too, caused by the limitations of the manufacturing process. However, the results are satisfactory, considering the intrinsic variability of the metallization and the substantial difference in terms of cost between the Flann horn and the printed one.

For the conformed-profile horn, the measured gain matches the simulated response with a remarkable accuracy, as shown in **Figure 32**. It presents a good behavior when compared with the Flann model as well, although some variations caused by manufacturing issues exist. However, they do not exceed 1.35 dB.

	E-plane		**H-plane**	
	Measured	**Simulated**	**Measured**	**Simulated**
Pyramidal horn	34°	33°	31.4°	30.7°
Conformed horn	24.8°	30.2°	28.6°	31.1°

Table 1. Simulated and measured 3-dB beamwidth.

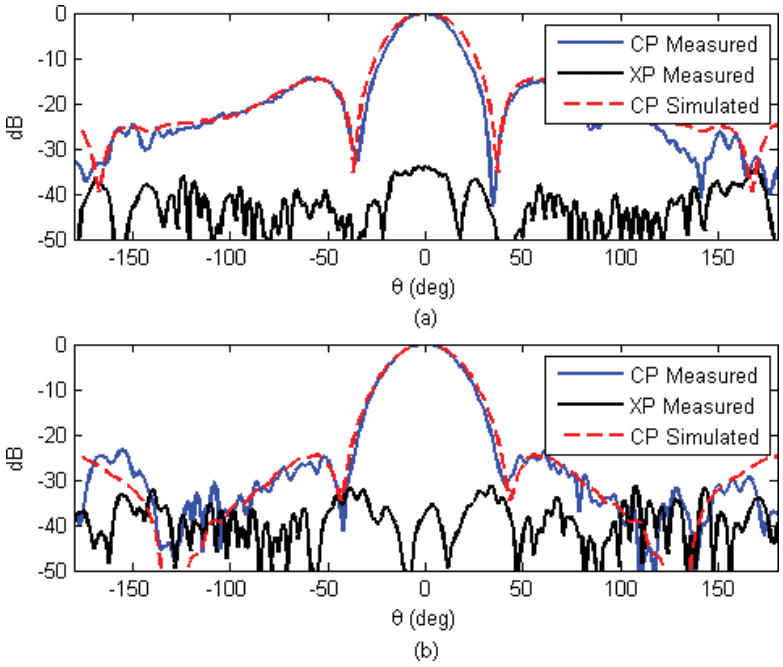

Figure 30. Normalized radiation pattern of the conformed-profile horn at frequency 12.5 GHz in (a) E-plane and (b) H-plane.

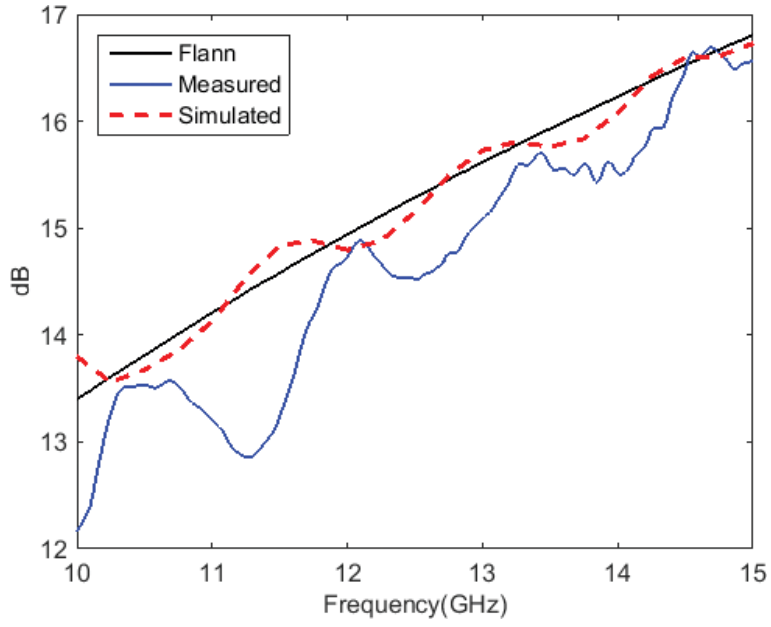

Figure 31. Pyramidal horn gain over broadband compared with simulation and commercial horn antenna from Flann.

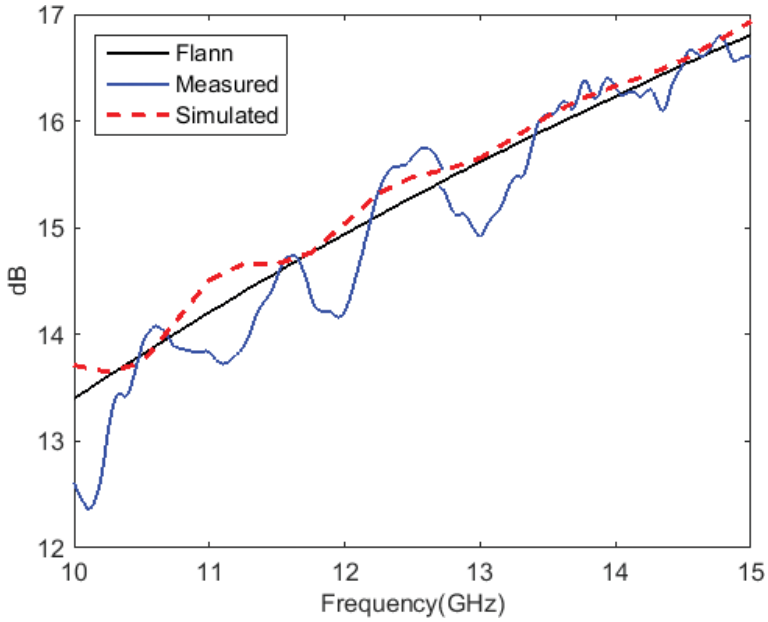

Figure 32. Conformed-profile horn gain over broadband compared with simulation and commercial horn antenna from Flann.

4. Conclusions

Although benefits of additive manufacturing are well known to the engineer community, its real application to a particular field needs a detailed analysis, even more when considering a low-cost perspective. With the work presented throughout this chapter, it can be concluded that low-cost 3D printing presents great advantages for the microwave engineer. The promptness to print models of great quality or to implement traditionally unfeasible geometries may be used for two main applications: prototyping and manufacturing of functional devices. Both applications may also increase the quality of microwave engineering education, especially for institutions without extraordinary resources.

In order to successfully address a low-cost 3D printing process in the microwave field, it is necessary to first take into account several key aspects: to set the maximum achievable working frequency, the best way to perform a metallization process, and the most suitable structure segmentation. This work has described all of them, emphasizing the best solutions as per authors' knowledge.

In addition, several prototypes of state-of-the art designs have been presented, together with real passive waveguide devices—individual filters, a diplexer, and a branch-line coupler—and two horn antennas. Experimental results have been discussed to evaluate their use in real-world applications. In general terms, the results agree quite well with the expected response, yet the discrepancies have also been explained.

In summary, additive manufacturing, and, in particular, its low-cost version, has a very promising future in the engineering field. Although further research is required—for instance, to enhance conductivity—it is a powerful tool worth to be discovered.

Acknowledgements

This work was supported in part by the Spanish government under grant TEC2016-76070-C3-1/2-R (ADDMATE, (AEI/FEDER, UE)) and the Comunidad de Madrid program S2013/ICE-3000 (SPADERADARCM).

The authors would like to thank Pablo Sanchez-Olivares for the gain and radiation pattern measurements at Escuela Politécnica Superior (Universidad Autónoma de Madrid).

Author details

Irene O. Saracho-Pantoja[1]*, José R. Montejo-Garai[1], Jorge A. Ruiz-Cruz[2] and Jesús M. Rebollar[1]

*Address all correspondence to: i.ortizdesaracho@alumnos.upm.es

1 Grupo de Electromagnetismo Aplicado, Information Processing and Telecommunications Center, Universidad Politécnica de Madrid, Madrid, Spain

2 Escuela Politécnica Superior, Universidad Autónoma de Madrid, Madrid, Spain

References

[1] Barnatt C. 3D Printing. 2nd ed; 2014

[2] Additive manufacturing—General principles—Terminology, ISO/ASTM 52900:2015 (ASTM F2792), 2015

[3] About Additive Manufacturing: The 7 Categories of Additive Manufacturing [Online], Loughborough University. Available: http://www.lboro.ac.uk/research/amrg/about/the7categoriesofadditivemanufacturing/

[4] Canessa E. Low-Cost 3D Printing for Science. International Centre for Theoretical Physics: Education & Sustainable Development; 2013

[5] RepRap, [Online]. Available: http://reprap.org

[6] Saracho-Pantoja IO. Ku band waveguide diplexer design for satellite communication. Implementation by additive manufacturing and experimental characterization; 2015. [Online]. Available: http://oa.upm.es/37345/

[7] Saracho-Pantoja IO, Montejo-Garai JR, Ruiz-Cruz JA, Rebollar JM. Low-cost additive manufacturing: A new approach to microwave waveguide engineering education through 3D printing. International Journal of Engineering Education. 2017;**33**(2(A)):741-750

[8] Montejo-Garai JR, Saracho-Pantoja IO, Ruiz-Cruz JA, Rebollar JM. Broadband and High-Purity Ku-Band Circular TE01-Mode Converter. New Delhi, India: Microwave Conference (APMC); 2016

[9] Montejo-Garai JR, Ruiz-Cruz JA, Leal-Sevillano CA, Rebollar JM, Roglá L, Sobrino S. Compact Low-Cost Diplexer with Elliptic Filter Response for Ka-Band Satellite Applications, 6th CNES/ESA International Workshop on Microwave Filters. France: Toulouse; 2015

[10] Loctite R3863 Circuit+. Available: http://www.loctite.es/

[11] Ferro-Silver Conductive Lacquer 6290 0341 (L204N), [Online]. Available: http://www.ferro.com

[12] RS Pro Conductive Adhesive [Online]. Available: http://uk.rs-online.com

[13] Matthaei GL, Young L, Jones EMT. Microwave Filters. Impedance-Matching Networks and Coupling Structures: McGraw-Hill Book Co.; 1964

[14] Graphit 33, Kontakt Chemie. Available: http://www.kontaktchemie.com/koc/KOCproductdetail.csp?division=&product=GRAPHIT%2033

[15] WR-62 Waveguide Load, Pasternack. Available: https://www.pasternack.com/waveguide-termination-frequency-range-1240-1800-ghz-pe6804-p.aspx

[16] Montejo-Garai J, Leal-Sevillano C, Ruiz-Cruz J, Rebollar J. Low-Cost Manufacturing by Fused Filament Fabrication of Microwave Waveguide Passive Devices for Space Applications, Workshop on Additive Manufacturing for Space Application. The Netherlands: Noordwijk; 2014

[17] Montejo-Garai J, Saracho-Pantoja I, Ruiz-Cruz J, Rebollar J. Design of Microwave Waveguide Devices for Space and Ground Applications Implemented by Additive Manufacturing, International Conference on Electromagnetics in Advanced Applications, Torino, Italy; 2015

[18] Ruiz-Cruz J, Montejo-Garai J, Rebollar J. Computer Aided Design of Waveguide Devices by Mode-Matching Methods. InTech: Passive Microwave Components and Antennas; 2010

[19] CST Microwave Studio, [Online]. Available: http://www.cst.com

[20] Pozar D. Microwave Engineering. Wiley; 2012

[21] Balannis C. Antenna Theory: Analysis and Design. Wiley; 2005

[22] Standard Gain Horn, Model 17240. Flann. Available: http://www.flann.com/products/antennas/